

Second-harmonic generation enhancement driven by quantum electron spill-out at metal surfaces

Muhammad Khalid* and Cristian Ciraci†

Istituto Italiano di Tecnologia, Center for Biomolecular Nanotechnologies, Via Barsanti 14, 73010 Arnesano, Italy.

(Dated: November 12, 2021)

Second-order nonlinear optical contributions originate from the angstrom-scale thin layer near the surface of centrosymmetric materials. At such length-scales quantum mechanical effects come into play and could be very crucial for an accurate description of a plasmonic system. In this article we develop a theoretical model based on the quantum hydrodynamic description to study free-electron nonlinear dynamics in plasmonic systems. Our model predicts strong resonances induced by the spill-out of electron density at the metal surface. We show that these resonances can boost second-harmonic generation efficiency up to 4 orders of magnitude and can be arbitrarily tuned by controlling the electron spill-out at the metal surface with the aid of thin dielectric layers. These results offer a possibility to artificially increase nonlinear susceptibilities by engineering optical properties at the quantum level.

INTRODUCTION

Modern photonic devices rely on nonlinear optical effects to carry out functionalities such as parametric tuning of the laser light spectrum, generation of ultra-short pulses, all-optical signal processing and ultra-fast switching^{1,2}. Furthermore, researchers are constantly extending the reach of nonlinear optical phenomena to a growing variety of practical applications, such as nonlinear microscopy³, ultrasensitive-optical shape characterization⁴, monitoring the processes in chemical synthesis of nanostructures⁵ and nonlinear plasmonic sensing⁶.

The inherent weakness of optical nonlinearities however has strongly hindered the chip integration of all-optical devices. Conventionally, to enhance the intrinsic nonlinear response of natural materials one has to rely on phase-matching or quasi-phase matching techniques, which require relatively long propagation distances. Distances can be shortened to several microns by employing photonic band-gap crystals, which is in general detrimental for the band width. A different route to increase nonlinear optical response can be achieved through plasmonic effects – collective oscillations of conduction electrons – whose near-field enhancement properties can effectively increase the nonlinear susceptibilities. Plasmons are not limited by diffraction and allow to focus the light in regions where dielectric nonlinearities can be embedded, or such that metallic nonlinearities themselves can be enhanced. The advantage of such approach is that one can effectively increase local nonlinear susceptibilities in nanoscale devices. The drawback however is that it is hard to combine building-up mechanisms that allow to increase the overall conversion efficiencies. In order to overcome this limitation then it is necessary to artificially increase nonlinear susceptibilities by engineering optical

properties at the quantum level. At THz frequencies, for example, this can be obtained using semiconductor quantum wells which are known to offer the largest nonlinear susceptibilities⁷. Increasing the carrier density however causes a transition from size-quantization to the classical regime of plasmon oscillations, in the visible range of frequencies.

In this article we show that quantum electron spill-out can be used to boost nonlinear efficiencies up to 4 orders of magnitude. In particular we focus on the process of second harmonic generation (SHG) in plasmonic systems. We develop a nonlinear quantum hydrodynamic theory that incorporates microscopic nonlinear electrodynamics and enables nonlinear optics calculations for realistic equilibrium density profiles.

Since the pioneering works on nonlinear optics^{8–11}, SHG has been continuously studied both experimentally^{12–20}, and theoretically^{21–31}. In centrosymmetric materials, such as noble metals, second-order nonlinearities in the bulk region are intrinsically forbidden³, nevertheless, the symmetry can be broken at the material surface, giving rise to a surface SHG mechanism^{32,33}. Typically, the SHG surface process occurs within a very thin layer of the order of few angstroms (a few Thomas-Fermi screening lengths) at the surface where the induced charges are confined. At such near-atomic length scales, classical electrodynamics fails to address the microscopic details and consideration of nonlocal and quantum mechanical effects may become crucial for accurately characterizing optical behavior of a metallic system.

In this context, the simplest tool dealing with nonlocal electron pressure is the Thomas-Fermi hydrodynamic theory (TFHT)^{34–40}. The TFHT is often combined with the hard-wall boundary condition, which overlooks the essential quantum mechanical effects like electron spill-out and quantum tunneling^{34–37,41}. While some efforts have been done to include in the hydrodynamic description space-dependent electron density profiles, such as linear and quadratic shape functions^{22–25}, the TFHT remains inadequate to deal with the realistic density pro-

* muhammad.khalid@iit.it

† cristian.ciraci@iit.it

file, as it yields spurious modes originating from the exponentially decaying tail of the density^{41,42}. The significance of an accurate description of the charge density profile in SHG has already been pointed out in the low-frequency regime both using a full quantum mechanical treatment^{27–31} as well as an orbital-free approach²⁶. Recently, a variety of methods based on effective local parameters have been proposed to deal with electron spill-out effects. These approaches are generally developed for the linear response regime^{43–45} and their generalization to the nonlinear dynamics is not trivial.

The TFHT on the other hand is intrinsically nonlinear and it has long been used to describe the nonlinear response of metals^{38–40}. In order to overcome its limitation, one should consider ∇n -dependent corrections (n being the electron density) to the free-electron gas kinetic energy, namely adding the von Weizsäcker term to the TF kinetic energy^{42,46,47}. Such approach is usually referred to as quantum hydrodynamic theory (QHT). Over the past few years, QHT has been applied to study linear optical properties of individual nanoparticles as well as of extremely coupled nanostructures (in the tunneling regime) and a very good agreement with the time-dependent density functional theory calculations has been reported^{42,47–49}. The QHT can also incorporate classical nonlinear effects, such as Lorentz and convective contributions, in multiscale plasmonic systems with deep sub-wavelength features, where the quantum effects cannot be neglected.

In the present work, we expand, for the first time, the QHT equations beyond the linear approximation and carry out its numerical implementation, which can be used to probe second-order nonlinearities in plasmonic structures of arbitrary shapes and sizes. In particular, we examine spectral dependence of SHG from Na and Ag thick films. First, by considering a smooth Na film, we show that the SHG efficiency spectra exhibit a strong resonance originating solely from the electron spill-out of electron density from the metal surface. We then compute SHG efficiency of a Ag film as a function of angle of incidence and compare results with the experimental data already reported in the literature¹⁸. In the spectral analysis, we notice that conversely to case of Na film, SHG from the Ag boundary does not show any resonance structure due to comparatively low electron spill-out and due to presence of background core permittivity. To step-up the electron spill-out, we coat the Ag film with a sub-wavelength thin dielectric layer and analyze its effect on SHG efficiency as compared to the bare film. Moreover, the impact of dielectric constant of the coating material is also discussed.

RESULTS

In QHT the pressure term takes the more general form of $\nabla \frac{\delta G[n]}{\delta n}$ where $G[n]$ is the energy functional of the free-

electron gas:

$$G[n] = T_{\text{TF}}[n] + \lambda T_{\text{W}}[n, \nabla n] + E_{\text{XC}}[n], \quad (1)$$

where $T_{\text{TF}}[n]$ is the TF kinetic energy functional, $T_{\text{W}}[n, \nabla n]$ is the gradient-dependent correction term (von Weizsäcker term) and $E_{\text{XC}}[n]$ is the exchange-correlation energy functional in the local density approximation. The parameter λ , weighting the von Weizsäcker functional, is of extreme importance as it defines the decay of the electron density and it is usually taken as $1/9 \leq \lambda \leq 1$ ⁴². The nonlinear QHT expansion up to second-order terms introduces three new groups of nonlinearities in addition to the classical nonlinear hydrodynamic terms^{50,51} (see the Methods section for more details): i) a new convective term, proportional to $\nabla n_0/n_0$, arising from the spatial dependence of the electron equilibrium density $n_0(\mathbf{r})$; ii) a quantum pressure term given by the product of the linear induced density n_1 and the gradient of the linear quantum pressure, i.e., $n_1 \nabla \left(\frac{\delta G[n]}{\delta n} \right)_1$; iii) a second-order quantum pressure term, $\nabla \left(\frac{\delta G[n]}{\delta n} \right)_2^{\text{NL}}$, that emerges from the nonlinear dependence of the kinetic functional from the electron density n . The last two terms generalize the nonlinear quantum pressure term in Refs. 50 and 51 and introduce a set of contributions that are inversely proportional to some powers of n_0 . Note that because $n_0 \rightarrow 0$ near the metal surface, these contributions, as well as the convective contributions, are expected to be important at the surface. Further details about the nonlinear QHT are reported in the Methods section and Supplementary Material S1.

We employ the nonlinear QHT to investigate the linear and second-order nonlinear optical properties of Na and Ag films, illuminated by a fundamental field with energy $E = \hbar\omega_1$ impinging at an angle θ_i with respect to the normal unit vector \hat{n} at the metal surface, as depicted in Fig. 1. We assume that the electric field is TM-polarized, i.e., laying in the incidence plane, as a TE-polarized wave would not induce any accumulation of charge at the metal interface. To make the system more realistic, we place the metal film on a glass substrate, although its impact on SHG is negligible for sufficiently thick films.

A simple Drude-like metal

Let us first consider a simple Drude-like metal system, a Na film placed in free space. Optical response of Na is easier to understand as the effect of interband transitions can be neglected at visible frequencies. We numerically analyze the spectral dependence of a 400 nm thick Na film excited by a TM-polarized plane wave. The self-consistent equilibrium charge density, calculated using Eq. (12) for different values the spill-out parameter λ (see the Methods section), is shown in Fig. 2a. $\lambda = 1/9$ is associated to a smaller spill-out and a faster decay of the electron density whereas $\lambda = 1/4$ represents a larger

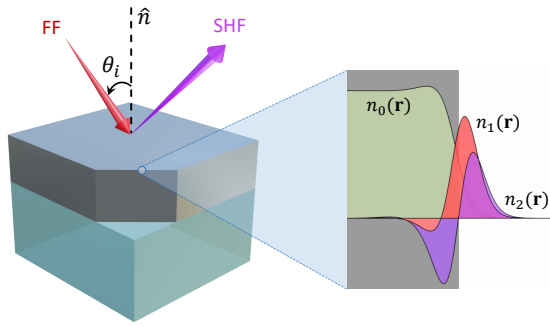


Figure 1. Schematic representation of the numerical setup for SHG. A thick metallic film placed on a glass substrate and illuminated by a TM-polarized plane wave making an angle θ_i with the unit normal vector \hat{n} . FF and SHF symbolize the fundamental field and the generated field at the SH, respectively. A zoom-in at the metal-air interface depicts spatial variation of the static and induced charges densities at the fundamental and second harmonics.

spill-out and a slower decay, as can be seen in the inset of Fig. 2a. The equilibrium density in case of TF approximation is also plotted. In this case electrons are not permitted to spill from the metal surface into the free space (hard-wall boundary condition). Since the impact of interband transitions in Na can be neglected, we set the core dielectric constant, $\varepsilon_\infty = 1$. In Fig. 2b we plot the linear reflection spectra. As expected, because of the absence of any structuring on the Na film surface, the TFHT does not present any particular feature. On the other hand, the spatial dependence of the charge density in the QHT produces a dip in the reflection spectra that depends on the equilibrium density decay rate at the metal-air interface. As the electron spill-out increases (for larger values of λ) the resonance dip moves to lower energies. This means that in principle by controlling the amount of electron spill-out from the metal surface, one could tune the resonance to the frequency of interest. These resonances are due to excitation of multipolar surface plasmons and are a consequence of electron spill-out exclusively. In the TF approximation (as well as in the standard local case not reported here) in fact, no resonant behavior can be observed. The existence of this multipolar collective mode was predicted several decades ago for sufficiently diffused electron density profiles⁵² and was also observed experimentally. The reader may refer to Ref. 53 and the references therein for a detailed overview of the theoretical and experimental studies of higher-order multipolar surface plasmons. These spill-out induced resonances can be exploited to enhance the SHG efficiency by several order of magnitude. The nonlinear QHT predicts in fact a very large enhancement of the SHG efficiency when the generated frequency matches the multipolar resonance in the linear spectrum. This kind of peak in the SHG intensity was also predicted in the nonlinear analysis of potassium

surface within the TFHT²⁵. Although, the authors in this work used unrealistic equilibrium density, nonetheless, they pointed out that the position and strength of this peak strongly depend on the shape of the charge density profile. Our QHT calculations show, as depicted in Fig. 2c, that SHG enhancement can exceed 4 orders of magnitude than the conversion efficiency away from resonance.

Fitting experimental data of SHG from Ag films

Simple Drude-like metals, such as Na, are convenient from a theoretical point of view since they present an ideal optical behavior. In practice however, they are very hard to work with because of their high reactivity. It would be interesting to analyze the possibility to observe a similar phenomenon in commonly used metals in plasmonics, such as noble metals. Noble metals' optical response is complicated by the contribution of the interband transitions, which can act on many levels. They modify the linear susceptibility, contribute to the nonlinear response⁵⁴ and affect both the equilibrium charge density and the induced charge distribution at the metal surface^{46,55,56}. In the following, we neglect the nonlinear contribution from interband transition and account for all the other effects by considering a polarizable medium of $\varepsilon_\infty > 1$ permeating the whole metal volume.

In order to evaluate the relevance of the nonlinear QHT model, we consider a smooth Ag film of 400 nm thickness, we account for core electrons' response with a local permittivity $\varepsilon_\infty = 5.9$ and compare the numerical results with experimental data already available in the literature¹⁸. The value of core permittivity $\varepsilon_\infty = 5.9$ was taken from Ref. 57 which was obtained by fitting the classical Drude model with the experimentally measured data. The SHG efficiency as a function of angle of incidence for different values of λ , computed within the full self-consistent nonlinear QHT, is compared against the experimental data as shown in Fig. 3a. It can be seen that for smaller λ (lower electron spill-out) the efficiency is largely underestimated. However, as the value of λ increases (eventually spill-out increases), the SHG efficiency steps up and for $\lambda = 1/2.5$ it coincides well with the peak of the data, although the angular dependence is not thoroughly reproduced. The experimental data shows a smooth angular dependence while the spectra predicted by the nonlinear QHT exhibit a minimum in the SHG efficiency in the range of 40°–50°. Although different from the measured data, this trend, and in particular the presence of a minimum, are in agreement with the time-dependent density functional theory calculations²⁸. In order to fit the experimental data, we introduce a phenomenological parameter α weighting the nonlinear part of the von Weizsäcker energy functional given in Eq. (1) such that:

$$\lambda T_W[n, \nabla n] = \lambda [T_W^L + \alpha T_W^{NL}], \quad (2)$$

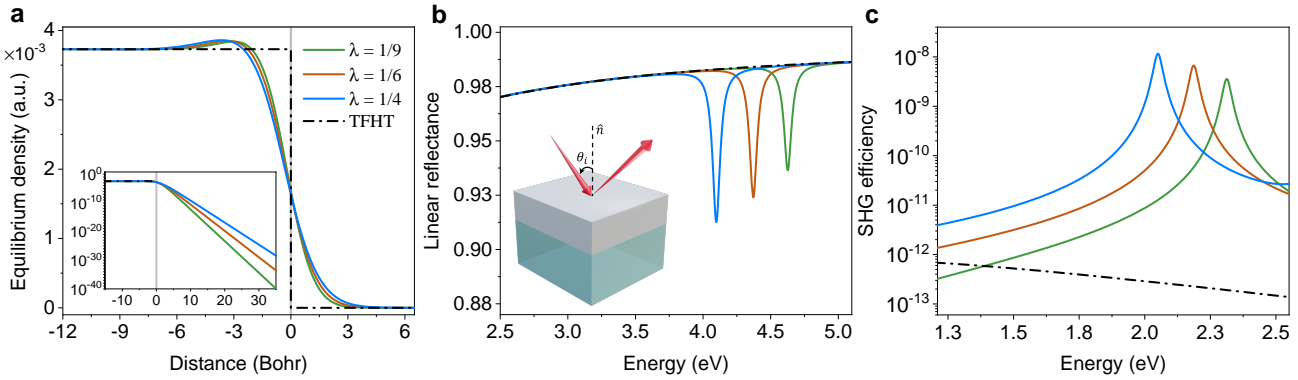


Figure 2. (a) Equilibrium electron density calculated self-consistently for different values of spill-out parameter λ . In TFHT a constant density inside the metal with no spatial dependence is assumed. The inset shows the decay of the electron density for each λ and the solid grey line indicates the position of the metal interface. (b) Linear reflectance and (c) SHG efficiency as a function of exciting (fundamental) energy of the incident field at $\theta_i = 75^\circ$ for different types of charge density profiles and $\gamma = 0.066$ eV.

where the superscripts L and NL indicate linear and nonlinear contributions, respectively. By properly choosing an optimal value of α the experimental data can be nicely approximated qualitatively as well as quantitatively for all angles of incidence. Figure 3b reports a comparison of the SHG efficiency between the experimental data and the nonlinear QHT when $\lambda = 1/4$ and $\alpha = 0.24 (= 1/4.15)$. The theory presented here can also approximate the experimental data for other values of λ provided that a suitable value of the parameter α is chosen (see Supplementary Material S2).

SHG resonances in Ag film with a dielectric coating

We have seen in the previous section that the Na films exhibit strong enhancement in the SHG spectra due to the presence of resonances induced by the electron density decays at the metal surface. Contrarily to the Na case however, we could not see any resonance structures neither in the linear nor in the SHG spectra for Ag films. The lack of such resonances is due to the combination of two factors. On the one hand, a larger ion density in Ag (smaller Wigner-Seitz radius) compared to Na, leads to a greater work function that keeps the electron tighter at the metal surface, producing a much smaller spill-out. As we have seen by varying λ , a faster decay of the electron density pushes the resonance to higher energies. On the other hand, the presence of a polarizable background in Ag (due to interband transitions) shifts the effective plasma frequency to lower energies. The result is that the Ag film becomes *transparent* before any multipolar resonance can be excited, completely suppressing the behavior observed for Na.

One possible way to circumvent this issue is to increase the electron spill-out from the Ag surface by reducing the work function at the metal interface. This can be obtained by modifying the dielectric environment sur-

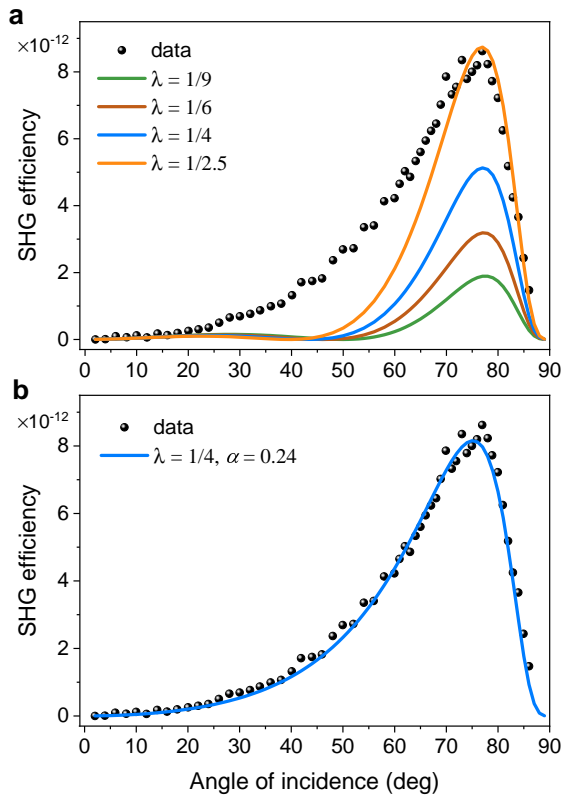


Figure 3. SHG efficiency as a function of angle of incidence from a 400 nm thick Ag film illuminated at $E = 1.17$ eV and considering $\gamma = 0.030$ eV; (a) for different values of the parameter λ and assuming $\alpha = 1$. (b) when $\lambda = 1/4$ and $\alpha = 0.24$. The results are compared against the experimental data taken from Ref. 18.

rounding the metal. In order to do so, we coat the film with a sub-wavelength thin layer of a dielectric material with a dielectric constant ϵ_r , as depicted in Fig. 4a. The linear reflectance and SHG efficiency spectra for a 400

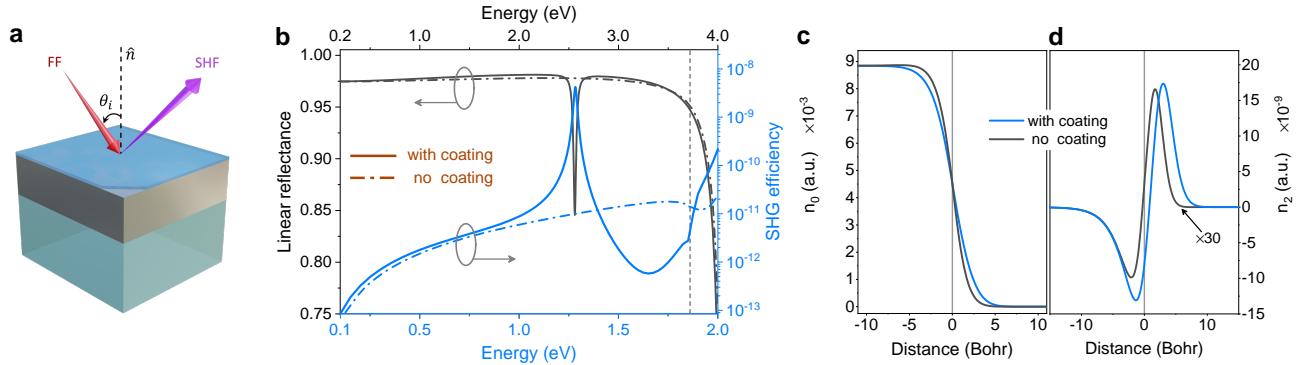


Figure 4. (a) Simulation setup for SHG from a Ag film coated with a sub-wavelength thin layer of a dielectric material and placed on a glass. (b) Linear reflectance and SHG efficiency from a 400 nm thick Ag film coated with 10 nm dielectric layer with $\epsilon_r = 5.9$ (solid lines) plotted at $\theta_i = 75^\circ$. The results for the Ag film without any coating are also shown for comparison (broken curves). The vertical dotted line represents the bulk plasma frequency (c) Self-consistent equilibrium density and (d) induced charge density at $E = 1.28$ eV for coated and uncoated films, plotted along the normal direction to the metal interface. The vertical solid grey line marks the metal interface.

nm Ag film, coated with 10 nm thick layer of a dielectric material with $\epsilon_r = \epsilon_\infty$ and placed on a glass substrate with refractive index $n = 1.45$, are plotted in Fig. 4b. Note that the figure also shows, for the sake of comparison, the spectra for the bare Ag film without any coating (as in Fig. 1). We observe that in the case of dielectric coating of Ag film, the linear response shows a dip in the reflectance which will result into a very strong resonance in the SHG efficiency, however, the Ag film without a coating does not show any resonance structure. This result is in fact very interesting as the spill-out induced resonances, which are suppressed in the commonly used setups in plasmonics, could be excited through a dielectric coating and, therefore, can be exploited for enhancing SHG. The equilibrium charge density of a Ag film with and without dielectric coating is plotted in Fig. 4c, which shows that due to presence of the dielectric coating the electron spill-out is more pronounced as compared to the uncoated slab. The dielectric material actually provides a channel for the electrons to escape from the metal surface and as a consequence of this higher spill-out the resonances can be observed in the linear and nonlinear spectra. Figure 4c presents the electron density at $\lambda = 1/4$ both for the coated and uncoated films, even if we consider $\lambda = 1$ for the uncoated case, the spill-out is still lower as compared to the coated case for $\lambda = 1/4$ (see Supplementary Material S3). The induced charge density at the SHG, plotted at $E = 1.28$ eV, for the coated and uncoated case is given in Fig. 4d. In both cases, the centroid of the charge density lies outside of the positive background edge. Although the spatial variation is quite similar, the induced charge density for the coated film is comparatively larger in width and magnitude, and is shifted farther away from the metal surface.

It is interesting to note that a similar behavior can be observed for different amount of the electron spill-out and it is not the product of a specific choice of parameters. In Figs. 5a and 5b we report linear and SHG spectra,

respectively, for the dielectric-coated Ag slab for different values of λ and compare results against the TFHT (with no spill-out). For each λ we observe a large resonance in SHG spectrum which is related to the dip in the corresponding linear reflectance. Neglecting the electron spill-out from the metal surface, as in the TFHT, prevents such features to appear neither in SHG nor in linear spectra. The SHG spectra of Fig. 5b display a noticeable minimum just before the peak resonance for each λ , which was not seen in the situation shown in Fig. 4b. To examine this feature, we consider $\lambda = 1/4$ and compute the SHG efficiency as a function of the angle of incidence and the fundamental energy for different values of α . We find that when $\alpha = 1$, there exists a minimum at almost all angles of incidence (Fig. 5c) whereas for $\alpha = 0.24$, there is no such minimum before the resonance, nevertheless, in this scenario a minimum also appears but after the resonance (Fig. 5d). In the latter case, the minimum is not present for all angles of incidence and since the spectrum shown in Fig. 4b was plotted at $\theta_i = 75^\circ$, therefore, no such minimum was detected there. This minimum in the SHG efficiency can be associated to the interplay between the different nonlinear contributions that involve the first order and second order terms of the von Weizsäcker energy functional respectively. While varying λ has a simultaneous effect on both terms, varying α modifies their respective weights, modifying the condition for which the two contributions cancel out.

So far we have fixed the refractive index of the coating material such that it corresponds to ϵ_∞ in order to reproduce a similar condition to Na where $\epsilon_\infty = 1$. It would be interesting at this point studying the influence of the dielectric constant of the coating material on the SHG efficiency. In Fig. 6 we report numerical results for linear response and SHG of the Ag film considering $\lambda = 1/4$, $\alpha = 0.24$ and various values of the dielectric constants ϵ_r of the coating material. The spectra for

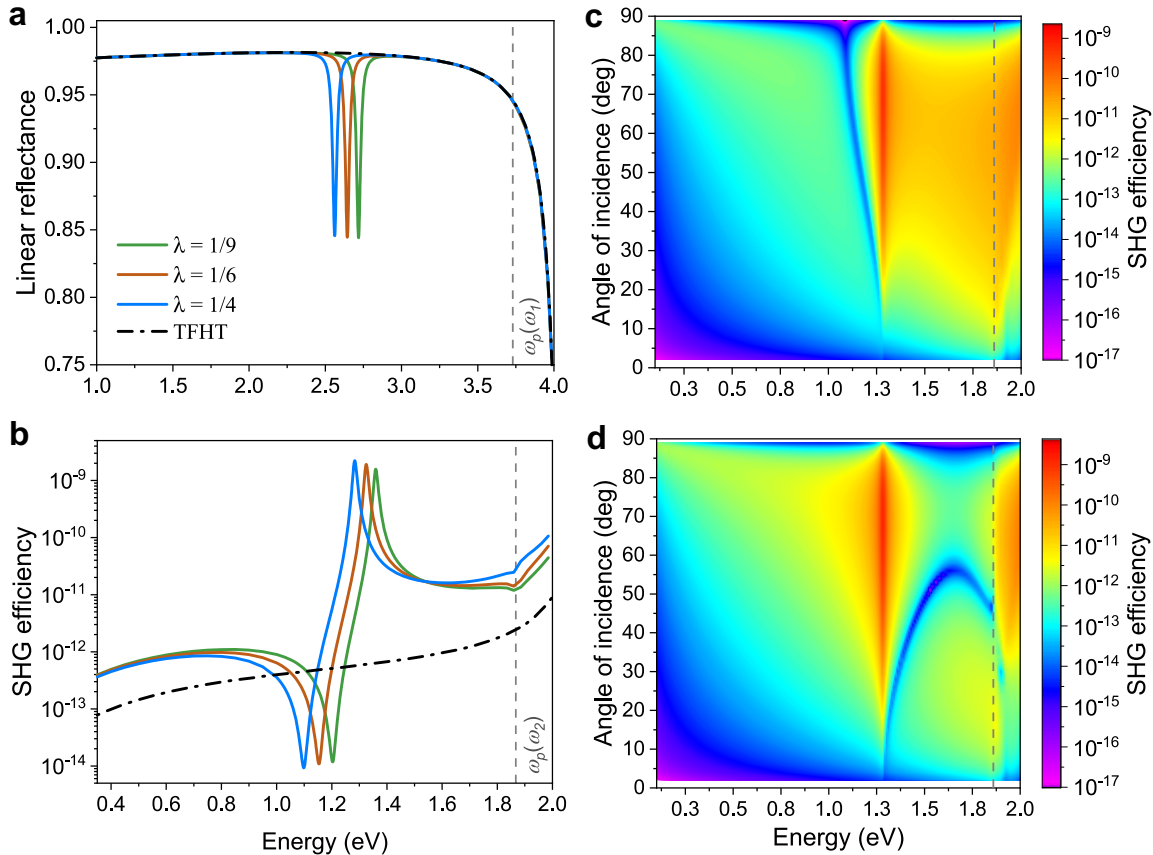


Figure 5. (a) Linear reflectance and (b) SHG efficiency from a dielectric-coated Ag film as a function of exciting energy (in eV) of the incident field for different values of the spill-out parameter λ and considering $\alpha = 1$. The results are compared against the TFHT spectra represented by the broken black lines. The vertical grey lines indicate the bulk plasma frequency at the fundamental and generated harmonic. The other parameters are the same as used in Fig. 4. SHG efficiency of the dielectric-coated Ag slab, for $\lambda = 1/4$ considering (c) $\alpha = 1$ and (d) $\alpha = 0.24$, plotted as a function of exciting energy and angle of incidence.

silver-air interface ($\varepsilon_r = 1$, i.e., without any coating) are also shown for completeness. Contrarily to the Ag-air interface, when $\varepsilon_r \neq 1$ a dip in the linear reflectance can be seen for each ε_r , although it becomes less intense for the smaller values of ε_r and completely disappears for $\varepsilon_r = 1$. This structure in the linear spectrum yields a large efficiency of the generated signal as depicted in Fig. 6b. It is interesting to note that as the value of dielectric constant of the coating layer increases, the resonance shifts towards the lower energies. This result, in fact, could be very important in many optical applications as the resonance of the SHG process can be tuned by coating the Ag film with a suitable dielectric material. A minimum in the SHG spectra for a lower value of the dielectric constants (with an exception of $\varepsilon_r = 1$) is also visible in the SHG spectra which appears after the resonance in the vicinity of bulk plasma frequency and corresponds to the similar situation as was discussed in Fig. 5. However, this minimum vanishes for the higher values of the dielectric constant.

DISCUSSION

We have presented a theoretical microscopic model to probe second-order nonlinearities at metal surfaces. Our approach was based on the QHT, which can efficiently handle the realistic profiles of the ground-state electron density. The nonlinear QHT predicts a very strong resonance in the SHG spectra that can boost the conversion efficiency by several orders of magnitude. This resonance shows a strong dependence on the spill-out of the electron density from the metal surface and is related to the excitation of multipolar surface plasmons in the linear response. Interestingly, these spill-out induced resonances can be tuned by controlling decay of the electron density from the metal surface with the aid of a dielectric coating. Moreover, excellent agreement with experimental data supports the concreteness of our results and their potential.

Our results suggest that an accurate description of the spatial variation of charge density at a metal surface is crucial in characterizing an accurate nonlinear

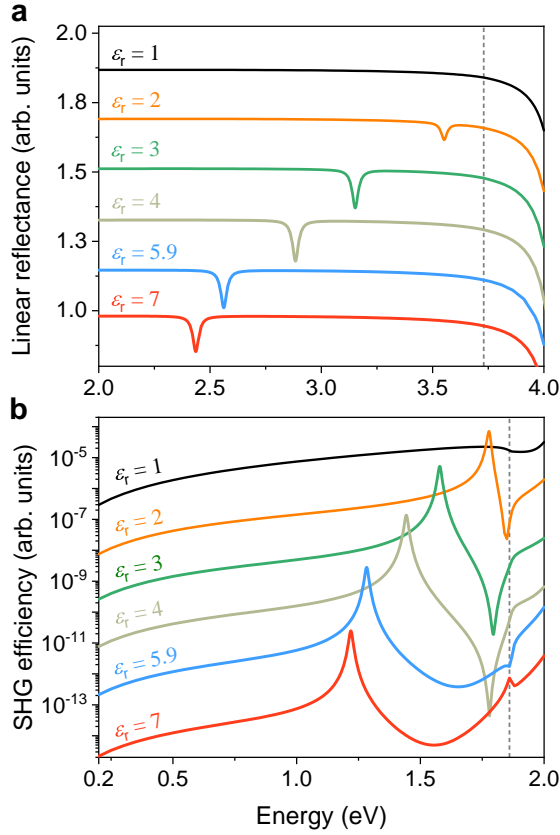


Figure 6. (a) Linear reflectance and (b) SHG efficiency as a function of exciting energy plotted at $\theta_i = 75^\circ$ for various values dielectric constant ϵ_r considered for the coating of Ag film. The result for the clean Ag film without any coating ($\epsilon_r = 1$) is also reported.

optical response. Although we have limited our study to films, the spill-out induced enhancement of SHG efficiency could be combined with plasmon-based field enhancement techniques to further increase nonlinear conversion rates. Moreover, because the nonlinear process is confined to the metal surface, such processes could be embedded in a hybrid metal-dielectric waveguide configuration that allows the build up of the nonlinear signals. We believe that the analysis presented in this article will be a source of motivation for further analytical and experimental research.

METHODS

Materials with very high density of free charges can be treated as charged fluids (in a positively charged background) and their optical properties can be characterized under the hydrodynamic description. The full nonlinear hydrodynamic equation of motion for an electronic system under the influence of electromagnetic fields \mathbf{E} and

\mathbf{B} can be expressed as⁴²:

$$m_e \left(\frac{\partial}{\partial t} + \mathbf{v} \cdot \nabla + \gamma \right) \mathbf{v} = -e (\mathbf{E} + \mathbf{v} \times \mathbf{B}) - \nabla \frac{\delta G[n]}{\delta n} \quad (3)$$

where m_e is the electron mass, \mathbf{v} is electron velocity field, γ is the damping rate and e is the absolute value of the electron charge; $n(\mathbf{r})$ represents the electron density and $G[n] = T_{TF}[n] + \lambda T_W[n, \nabla n] + E_{XC}[n]$ is the energy functional incorporating the TF kinetic energy, the gradient-dependent correction term and the exchange-correlation energy functional respectively. In specifying the energy functionals in Eq. (1) we do not include the effect of non-local broadening (see Ref. 47 for more details) to avoid the further numerical complexity. Considering the electron current $\mathbf{J} = -nev$, Eq. (3) can expressed as:

$$\frac{\partial \mathbf{J}}{\partial t} + \gamma \mathbf{J} = \frac{e^2 n}{m_e} \mathbf{E} - \frac{e}{m_e} \mathbf{J} \times \mathbf{B} + \frac{en}{m_e} \nabla \frac{\delta G[n]}{\delta n} + \frac{1}{e} \left(\frac{\mathbf{J}}{n} \nabla \cdot \mathbf{J} - \mathbf{J} \cdot \nabla \frac{\mathbf{J}}{n} \right). \quad (4)$$

A similar equation can also be directly derived from the single-particle Kohn-Sham equation⁴⁷.

We proceed by writing the fields as the sum of few harmonics:

$$n(\mathbf{r}, t) = n_0(\mathbf{r}) + n_1(\mathbf{r})e^{-i\omega_1 t} + n_2(\mathbf{r})e^{-i\omega_2 t} + \text{c.c.} \quad (5)$$

$$\mathbf{E}(\mathbf{r}, t) = \mathbf{E}_0(\mathbf{r}) + \mathbf{E}_1(\mathbf{r})e^{-i\omega_1 t} + \mathbf{E}_2(\mathbf{r})e^{-i\omega_2 t} + \text{c.c.} \quad (6)$$

$$\mathbf{J}(\mathbf{r}, t) = \mathbf{J}_1(\mathbf{r})e^{-i\omega_1 t} + \mathbf{J}_2(\mathbf{r})e^{-i\omega_2 t} + \text{c.c.} \quad (7)$$

$$\mathbf{B}(\mathbf{r}, t) = \mathbf{B}_1(\mathbf{r})e^{-i\omega_1 t} + \mathbf{B}_2(\mathbf{r})e^{-i\omega_2 t} + \text{c.c.} \quad (8)$$

where $\omega_2 = 2\omega_1$ and \mathbf{E}_0 and n_0 represent the steady-state electric field and ground-state electron density. The subscripts 1 and 2 indicate the field quantities at the fundamental and the second harmonic, respectively. Assuming the undepleted pump approximation, that is, the fundamental field is not affected by the conversion process, and recalling that $\mathbf{J} = \dot{\mathbf{P}}$, in view of Eqs. (5)-(8), Eq. (4) results into following set of equations:

$$-\frac{en_0}{m_e} \nabla \left(\frac{\delta G[n]}{\delta n} \right)_1 - (\omega_1^2 + i\gamma\omega_1) \mathbf{P}_1 = \epsilon_0 \omega_p^2 \mathbf{E}_1 \quad (9)$$

$$-\frac{en_0}{m_e} \nabla \left(\frac{\delta G[n]}{\delta n} \right)_2 - (\omega_2^2 + i\gamma\omega_2) \mathbf{P}_2 = \epsilon_0 \omega_p^2 \mathbf{E}_2 + \mathbf{S}_{NL} \quad (10)$$

where $\omega_p(\mathbf{r}) = \sqrt{e^2 n_0(\mathbf{r}) / (m_e \epsilon_0)}$ is the space-dependent plasma frequency and the nonlinear source term is:

$$\begin{aligned} \mathbf{S}_{NL} = & \frac{e^2 n_1}{m_e} \mathbf{E}_1 + i\omega_1 \frac{\mu_0 e}{m_e} \mathbf{P}_1 \times \mathbf{H}_1 + \\ & - \frac{\omega_1^2}{en_0} \left(\mathbf{P}_1 \nabla \cdot \mathbf{P}_1 + \mathbf{P}_1 \cdot \nabla \mathbf{P}_1 - \mathbf{P}_1 \cdot \mathbf{P}_1 \frac{\nabla n_0}{n_0} \right) + \\ & + \frac{en_1}{m_e} \nabla \left(\frac{\delta G[n]}{\delta n} \right)_1 + \frac{en_0}{m_e} \nabla \left(\frac{\delta G[n]}{\delta n} \right)_2 \end{aligned} \quad (11)$$

Mathematical expressions for the linear potentials $\left(\frac{\delta G[n]}{\delta n}\right)_{1,2}$ are reported in detail in Ref. 42 whereas expressions for the nonlinear potentials are derived in the Supplementary Material S1. In addition to the classical nonlinear hydrodynamic terms^{50,51}, i.e., Coulomb, Lorentz and convective terms (note that there is one extra convective term, $\propto \nabla n_0/n_0$, arising from the spatial dependence of the electron density), two new quantum terms emerge as discussed in the Results section.

In implementing our nonlinear QHT we follow the jellium approximation⁵⁸, which assumes that the electrons in a metal are confined by a constant positive background charge $n^+ = (\frac{4}{3}\pi r_s^3)^{-1}$, where r_s indicates the Wigner-Seitz radius ($r_s = 4$ for Na and $r_s = 3$ for Ag). The space-dependent equilibrium charge density can be calculated by combining the zero-*th* order QHT equation with the Gauss's law, which leads to the following nonlinear static equation⁴⁷:

$$\nabla \varepsilon_\infty(\mathbf{r}) \cdot \nabla \left(\frac{\delta G}{\delta n} \right)_{n=n_0} + \frac{e^2}{\varepsilon_0} (n_0 - n^+) = 0 \quad (12)$$

where ε_0 symbolizes permittivity of free-space. ε_∞ is the core dielectric constant presenting a local contribution to

the metal permittivity. We solve Eqs. (9), (10) and (12) coupled to two frequency-dependent wave equations in a finite-element-method based numerical simulator COMSOL Multiphysics⁵⁹, which offers quite flexible implementation of these expressions. Numerical implementation of these equations is given in the Supplementary Material S4.

ACKNOWLEDGMENTS

C. C. thanks Prof. John Sipe for valuable insights and discussions. The authors thank the Air Force Office of the Scientific Research for supporting this work under the award number FA9550-17-1-0177.

AUTHOR CONTRIBUTIONS

C.C. developed the theory; M.K. set up the numerical model and performed the simulations; C.C. and M.K. analyzed the numerical data and wrote the manuscript; C.C. supervised the project.

[1] E. Sidick, A. Knoesen, and A. Dienes, *Opt. Lett.* **19**, 266 (1994).
[2] A. V. Krasavin, P. Ginzburg, and A. V. Zayats, *Laser & Photonics Reviews* **12**, 1700082 (2018).
[3] R. W. Boyd, *Nonlinear Optics*, 3rd ed. (Academic Press, Inc., USA, 2008).
[4] J. Butet, K. Thyagarajan, and O. J. F. Martin, *Nano Lett.* **13**, 1787 (2013).
[5] C. Sauerbeck, M. Haderlein, B. Schüller, B. Braunschweig, W. Peukert, and R. N. Klupp Taylor, *ACS Nano* **8**, 3088 (2014).
[6] J. Butet and O. J. F. Martin, *Nanoscale* **6**, 15262 (2014).
[7] J. Lee, M. Tymchenko, C. Argyropoulos, P.-Y. Chen, F. Lu, F. Demmerle, G. Boehm, M.-C. Amann, A. Alù, and M. A. Belkin, *Nature* **511**, 65 (2014).
[8] R. W. Terhune, P. D. Maker, and C. M. Savage, *Phys. Rev. Lett.* **8**, 404 (1962).
[9] F. Brown, R. E. Parks, and A. M. Sleeper, *Phys. Rev. Lett.* **14**, 1029 (1965).
[10] S. S. Jha, *Phys. Rev.* **140**, A2020 (1965).
[11] N. Bloembergen and Y. R. Shen, *Phys. Rev.* **141**, 298 (1966).
[12] H. Sonnenberg and H. Heffner, *J. Opt. Soc. Am.* **58**, 209 (1968).
[13] H. J. Simon, D. E. Mitchell, and J. G. Watson, *Phys. Rev. Lett.* **33**, 1531 (1974).
[14] J. C. Quail and H. J. Simon, *Phys. Rev. B* **31**, 4900 (1985).
[15] J. L. Coutaz, D. Maystre, M. Nevière, and R. Reinisch, *Journal of Applied Physics* **62**, 1529 (1987).
[16] C. Chang and J. Lue, *Surface Science* **393**, 231 (1997).
[17] D. Krause, C. W. Teplin, and C. T. Rogers, *Journal of Applied Physics* **96**, 3626 (2004).
[18] K. A. O'Donnell and R. Torre, *New J. Phys.* **7**, 154 (2005).
[19] N. B. Grosse, J. Heckmann, and U. Woggon, *Phys. Rev. Lett.* **108**, 136802 (2012).
[20] M. Galanty, O. Shavit, A. Weissman, H. Aharon, D. Gachet, E. Segal, and A. Salomon, *Light Sci Appl* **7**, 49 (2018).
[21] J. Rudnick and E. A. Stern, *Phys. Rev. B* **4**, 4274 (1971).
[22] J. E. Sipe, V. C. Y. So, M. Fukui, and G. I. Stegeman, *Phys. Rev. B* **21**, 4389 (1980).
[23] J. Sipe, V. So, M. Fukui, and G. Stegeman, *Solid State Communications* **34**, 523 (1980).
[24] M. Corvi and W. L. Schaich, *Phys. Rev. B* **33**, 3688 (1986).
[25] J. A. Maytorena, W. L. Mochán, and B. S. Mendoza, *Phys. Rev. B* **51**, 2556 (1995).
[26] A. Chizmeshya and E. Zaremba, *Phys. Rev. B* **37**, 2805 (1988).
[27] M. Weber and A. Liebsch, *Phys. Rev. B* **35**, 7411 (1987).
[28] A. Liebsch, *Phys. Rev. Lett.* **61**, 1233 (1988).
[29] C. D. Hu, *Phys. Rev. B* **40**, 7520 (1989).
[30] T. HEINZ, in *Nonlinear Surface Electromagnetic Phenomena*, Modern Problems in Condensed Matter Sciences, Vol. 29, edited by H.-E. PONATH and G. STEGEMAN (Elsevier, 1991) pp. 353 – 416.
[31] W. L. Schaich, *Phys. Rev. B* **61**, 10478 (2000).
[32] R. Vollmer, M. Straub, and J. Kirschner, *Surface Science* **352-354**, 684 (1996).
[33] J. Butet, P.-F. Brevet, and O. J. F. Martin, *ACS Nano* **9**, 10545 (2015).
[34] C. Ciraci, R. T. Hill, J. J. Mock, Y. Urzhumov, A. I. Fernandez-Dominguez, S. A. Maier, J. B. Pendry, A. Chilkoti, and D. R. Smith, *Science* **337**, 1072 (2012).

[35] C. Ciracì, J. B. Pendry, and D. R. Smith, *ChemPhysChem* **14**, 1109 (2013).

[36] S. Raza, S. I. Bozhevolnyi, M. Wubs, and N. Asger Mortensen, *J. Phys.: Condens. Matter* **27**, 183204 (2015).

[37] D. Yoo, F. Vidal-Codina, C. Ciracì, N.-C. Nguyen, D. R. Smith, J. Peraire, and S.-H. Oh, *Nat Commun* **10**, 4476 (2019).

[38] X. M. Hua and J. I. Gersten, *Phys. Rev. B* **33**, 3756 (1986).

[39] C. Ciracì, M. Scalora, and D. R. Smith, *Phys. Rev. B* **91**, 205403 (2015).

[40] M. Scalora, M. A. Vincenti, D. de Ceglia, N. Akozbek, M. J. Bloemer, C. De Angelis, J. W. Haus, R. Vilaseca, J. Trull, and C. Cojocaru, *Phys. Rev. A* **98**, 023837 (2018).

[41] W. Yan, *Phys. Rev. B* **91**, 115416 (2015).

[42] C. Ciracì and F. Della Sala, *Phys. Rev. B* **93**, 205405 (2016).

[43] R. Esteban, A. G. Borisov, P. Nordlander, and J. Aizpuru, *Nat Commun* **3**, 825 (2012).

[44] W. Yan, M. Wubs, and N. Asger Mortensen, *Phys. Rev. Lett.* **115**, 137403 (2015).

[45] M. Kupresak, X. Zheng, G. A. E. Vandenbosch, and V. V. Moshchalkov, *Adv. Theory Simul.* **1**, 1800076 (2018).

[46] G. Toscano, J. Straubel, A. Kwiatkowski, C. Rockstuhl, F. Evers, H. Xu, N. Asger Mortensen, and M. Wubs, *Nat Commun* **6**, 7132 (2015).

[47] C. Ciracì, *Phys. Rev. B* **95**, 245434 (2017).

[48] M. Khalid, F. D. Sala, and C. Ciracì, *Opt. Express* **26**, 17322 (2018).

[49] M. Khalid and C. Ciracì, *Photonics* **6**, 39 (2019).

[50] M. Scalora, M. A. Vincenti, D. de Ceglia, V. Roppo, M. Centini, N. Akozbek, and M. J. Bloemer, *Phys. Rev. A* **82**, 043828 (2010).

[51] C. Ciracì, E. Poutrina, M. Scalora, and D. R. Smith, *Phys. Rev. B* **86**, 115451 (2012).

[52] A. J. Bennett, *Phys. Rev. B* **1**, 203 (1970).

[53] J. M. Pitkarke, V. M. Silkin, E. V. Chulkov, and P. M. Echenique, *Rep. Prog. Phys.* **70**, 1 (2007).

[54] M. Scalora, M. A. Vincenti, D. de Ceglia, and J. W. Haus, *Phys. Rev. A* **90**, 013831 (2014).

[55] T. V. Teperik, P. Nordlander, J. Aizpurua, and A. G. Borisov, *Phys. Rev. Lett.* **110**, 263901 (2013).

[56] A. Liebsch, *Phys. Rev. B* **57**, 3803 (1998).

[57] M. Moaied, S. Palomba, and K. Ostrikov, *J. Opt.* **19**, 105402 (2017).

[58] M. Brack, *Rev. Mod. Phys.* **65**, 677 (1993).

[59] COMSOL Multiphysics, <https://www.comsol.com>.

Supplementary Material: Second-harmonic generation enhancement driven by quantum electron spill-out at metal surfaces

Muhammad Khalid* and Cristian Ciraci†

Istituto Italiano di Tecnologia, Center for Biomolecular Nanotechnologies, Via Barsanti 14, 73010 Arnesano, Italy.

(Dated: November 12, 2021)

S1. NONLINEAR TERMS OF $G[n]$

Recalling the energy functional $G[n]$, representing the total internal energy of an electronic system (see Eq. (1) in the main text),

$$G[n] = T_{\text{TF}}[n] + \lambda T_{\text{W}}[n, \nabla n] + E_{\text{XC}}[n], \quad (\text{S1})$$

Here we report derivation of the nonlinear terms of the energy functionals appearing in the above equation. The functional derivative of the terms in Eq. (S1) can be expressed as¹,

$$\frac{\delta T_{\text{TF}}}{\delta n} = (E_h a_0^2) \frac{5}{3} c_{\text{TF}} n^{2/3}, \quad (\text{S2})$$

$$\frac{\delta T_{\text{W}}}{\delta n} = (E_h a_0^2) \frac{1}{8} \left(\frac{\nabla n \cdot \nabla n}{n^2} - 2 \frac{\nabla^2 n}{n} \right), \quad (\text{S3})$$

$$\frac{\delta E_{\text{xc}}}{\delta n} = \varepsilon_{\text{xc}} + n \frac{d\varepsilon_{\text{xc}}}{dn}, \quad (\text{S4})$$

where,

$$\varepsilon_{\text{xc}} = -c_{\text{x}} n^{1/3} + \varepsilon_{\text{c}} \quad (\text{S5})$$

$$\varepsilon_{\text{c}} = \begin{cases} a \ln r_s + b + c r_s \ln r_s + d r_s, & r_s < 1 \\ \frac{\gamma}{1 + \beta_1 r_s^{1/2} + \beta_2 r_s}, & r_s \geq 1 \end{cases} \quad (\text{S6})$$

and $E_h = \frac{\hbar^2}{m_e a_0^2}$ is the Hartree energy, a_0 represents the Bohr radius, $c_{\text{TF}} = \frac{3}{10} (3\pi^2)^{1/3}$ and $c_{\text{x}} = \frac{3}{4} (\frac{3}{\pi})^{1/3}$. The coefficients appearing in Eq. (S6) are given in Ref. 1. Electron density as the sum of few harmonics can be expressed as:

$$n = n_0 + \sum_j n_j e^{-i\omega_j t} + \text{c.c.}, \quad \text{where, } j = 1, 2 \quad (\text{S7})$$

For mathematical convenience, dropping the summation operator and writing the above equation simply as:

$$n = n_0 + n_j e^{-i\omega_j t} \quad (\text{S8})$$

Second-order contribution of $\frac{\delta T_{\text{TF}}}{\delta n}$ can be obtained by substituting Eq. (S8) into Eq. (S2) and applying the Binomial expansion, we get,

$$\frac{\delta T_{\text{TF}}}{\delta n} = (E_h a_0^2) \frac{5}{3} C_{\text{TF}} \left[n_0^{2/3} + \frac{2}{3} n_0^{-1/3} (n_j e^{-i\omega_j t}) - \frac{1}{9} n_0^{-4/3} (n_j e^{-i\omega_j t})^2 + \text{c.c.} + \dots \right], \quad (\text{S9})$$

Focusing only on the second-order terms and neglecting the higher harmonics ($\omega > \omega_2$), we are left with:

$$\left(\frac{\delta T_{\text{TF}}}{\delta n} \right)_2^{\text{NL}} = -\frac{5}{27} C_{\text{TF}} n_0^{-3/4} n_1^2 \quad (\text{S10})$$

*Electronic address: muhammad.khalid@iit.it

†Electronic address: cristian.ciraci@iit.it

Now, the nonlinear terms due to T_W can be derived by inserting (S8) into (S3), as:

$$\frac{\delta T_W}{\delta n} = (E_h a_0^2) \frac{1}{8} \left[\frac{\nabla (n_0 + n_j e^{-i\omega_j t}) \cdot \nabla (n_0 + n_j e^{-i\omega_j t})}{(n_0 + n_j e^{-i\omega_j t})^2} - 2 \frac{\nabla^2 (n_0 + n_j e^{-i\omega_j t})}{n_0 + n_j e^{-i\omega_j t}} \right] \quad (\text{S11})$$

Expanding $(n_0 + n_j e^{-i\omega_j t})^{-2}$ in the above equation and doing some algebra results in the following nonlinear contribution:

$$\left(\frac{\delta T_W}{\delta n} \right)_2^{\text{NL}} = \frac{\nabla n_1 \cdot \nabla n_1}{n_0^2} - 4 \frac{\nabla n_0 \cdot \nabla n_1}{n_0^3} n_1 + 2 \frac{\nabla^2 n_1}{n_0^2} n_1 + 3 \frac{|\nabla n_0|^2}{n_0^4} n_1^2 - 2 \frac{\nabla^2 n_0}{n_0^3} n_1^2, \quad (\text{S12})$$

Similarly, the nonlinear terms for exchange-correlation potential can be obtained by using (S8) into (S4), resulting in the following expression:

$$\left(\frac{\delta E_{\text{xc}}}{\delta n} \right)_2^{\text{NL}} = \frac{1}{2} \left(3 \frac{d^2 \epsilon_{\text{x}}}{dn^2} + n \frac{d^3 \epsilon_{\text{x}}}{dn^3} + 3 \frac{d^2 \epsilon_{\text{c}}}{dn^2} + n \frac{d^3 \epsilon_{\text{c}}}{dn^3} \right)_{n=n_0} n_1^2 \quad (\text{S13})$$

where,

$$\begin{aligned} \frac{d^2 \epsilon_{\text{x}}}{dn^2} &= \frac{2}{9} C_{\text{x}} n^{-5/3}, \\ \frac{d^3 \epsilon_{\text{x}}}{dn^3} &= \frac{10}{27} C_{\text{x}} n^{-8/3}, \\ \frac{d^2 \epsilon_{\text{c}}}{dn^2} &= \begin{cases} \frac{1}{3} \left[\frac{r_s}{3} (5c + 4d + 4\text{clnr}_s) + a \right] n^{-2}, & r_s < 1 \\ \frac{\gamma}{9} \left[\frac{\frac{7\beta_1}{4} r_s^{1/2} + 4\beta_2 r_s}{(1 + \beta_1 r_s^{1/2} + \beta_2 r_s)^2} + \frac{(\frac{\beta_1}{2} r_s^{1/2} + \beta_2 r_s)^2}{(1 + \beta_1 r_s^{1/2} + \beta_2 r_s)^4} \right] n^{-2}, & r_s \geq 1 \end{cases} \\ \frac{d^3 \epsilon_{\text{c}}}{dn^3} &= \begin{cases} -\frac{1}{9} \left[(13c + \frac{28}{3}d + \frac{28}{3}\text{clnr}_s) r_s + 6a \right] n^{-3}, & r_s < 1 \\ \frac{\gamma}{9} \left[\frac{\frac{7\beta_1}{2} r_s^{1/2} + 8\beta_2 r_s}{(1 + \beta_1 r_s^{1/2} + \beta_2 r_s)^2} + \frac{\frac{7}{24} \beta_1 r_s^{1/2} + \frac{4}{3} \beta_2 r_s - \frac{7}{24} \beta_1 r_s - \frac{7}{8} \beta_1 \beta_2 r_s^{2/3} - \frac{4}{3} \beta_2^2 r_s^2}{(1 + \beta_1 r_s^{1/2} + \beta_2 r_s)^4} + \right. \\ \left. + \frac{2 \left(\frac{\beta_1}{2} r_s^{1/2} + \beta_2 r_s \right)^2}{(1 + \beta_1 r_s^{1/2} + \beta_2 r_s)^4} - \frac{\left(\frac{\beta_1}{2} r_s^{1/2} + \beta_2 r_s \right) \left(-\frac{1}{6} \beta_1 r_s - \frac{2}{3} \beta_2 r_s + \frac{1}{6} \beta_1^2 r_s + \frac{1}{2} \beta_1 \beta_2 r_s^{3/2} + \frac{2}{3} \beta_2^2 r_s^2 \right)}{(1 + \beta_1 r_s^{1/2} + \beta_2 r_s)^5} \right] n^{-3}, & r_s \geq 1 \end{cases} \end{aligned}$$

S2. APPROXIMATING EXPERIMENTAL DATA FOR DIFFERENT λ

The nonlinear quantum hydrodynamic theory can also approximate the experimental data² for Ag film for a given λ , representing the electron spill-out from metal surface provided that the value of the parameter α , weighting the nonlinear part of the von-Weizsäcker energy functional (see Eq. (2) in the main text), is properly chosen. Figure S1 plots the SHG efficiency for a clean Ag film computed with the nonlinear QHT and compared against the experimental results.

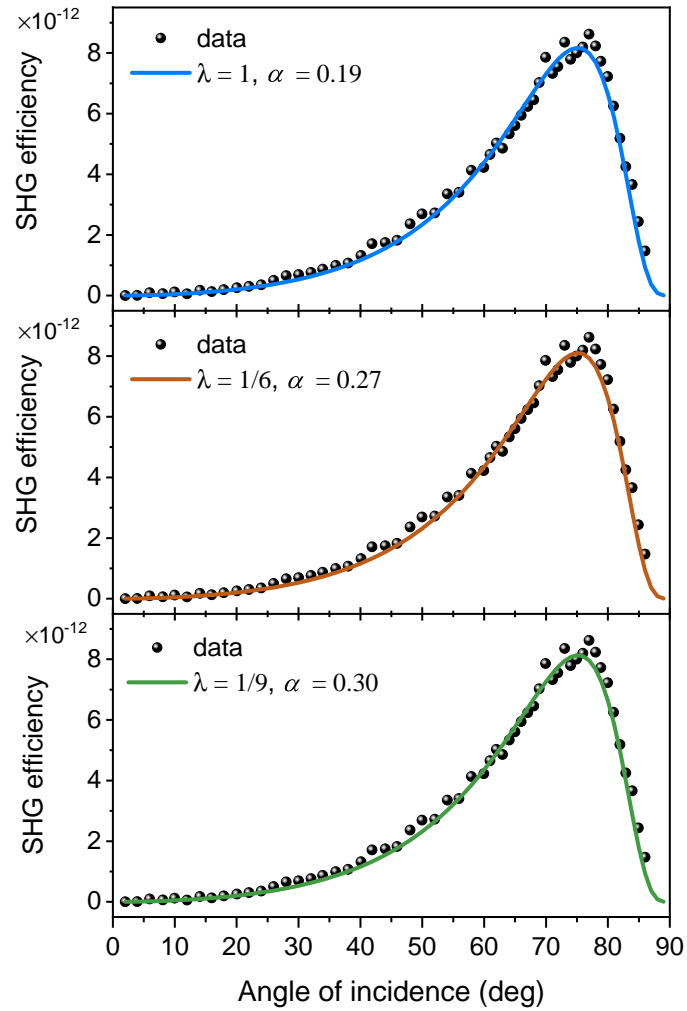


Figure S1: Nonlinear QHT approximating the experimental data² for a 400 nm thick clean Ag film excited by a TM-polarized plane wave at $E = 1.17$ eV, considering different values of λ and the parameter α weighting the nonlinear von-Weizsäcker energy functional.

S3. EQUILIBRIUM CHARGE DENSITY FOR COATED AND UNCOATED AG FILMS

Here we compare the ground-state electron density of the uncoated Ag film considering different values of spill-out parameter λ against the dielectric-coated Ag film for $\lambda = 1/4$. It can be seen that for uncoated film even for $\lambda = 1$ the spill-out is relatively lower as compared to the coated film for $\lambda = 1/4$, as shown in Fig. S2.

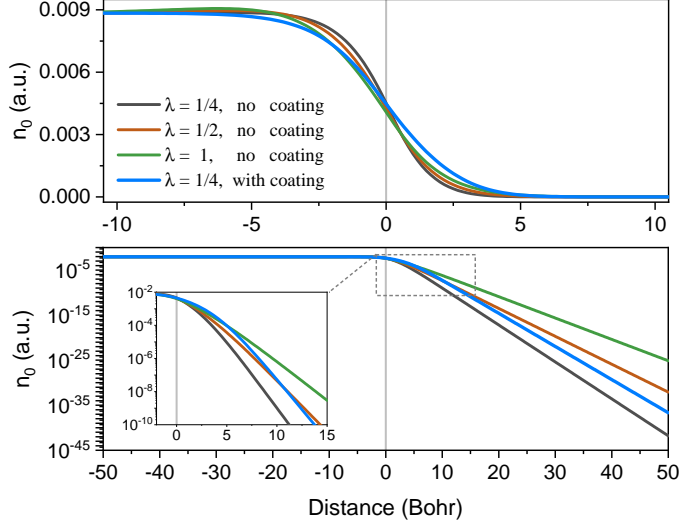


Figure S2: Equilibrium electron density for a neat Ag film by considering different values of λ and compared with the density of the coated film for $\lambda = 1/4$, considering dielectric constant of the coating material $\varepsilon_r = \varepsilon_\infty$. The lower panel shows the decay of the density.

S4. WEAK FORMULATION

In FEM based approaches the differential equations are usually expressed in their weak form to relax the continuity requirements for the test functions. We numerically implement Eqs. (9)–(11) of the main text and two frequency-dependent wave equations in FEM-based solver COMSOL Multiphysics³. In the following we derive the weak formulation of these equations. Re-writing Eqs. (9) and (10) in a compact form,

$$-\frac{en_0}{m_e} \nabla \left(\frac{\delta G[n]}{\delta n} \right)_j - (\omega_j^2 + i\gamma\omega_j) \mathbf{P}_j = \varepsilon_0 \omega_p^2 \mathbf{E}_j + \mathbf{S}_j, \quad \text{where, } j = 1, 2 \quad (\text{S14})$$

where $\mathbf{S}_1 = 0$ and $\mathbf{S}_2 = \mathbf{S}_{\text{NL}}$, given by Eq. (11):

$$\begin{aligned} \mathbf{S}_{\text{NL}} = & \frac{e^2 n_1}{m_e} \mathbf{E}_1 + i\omega_1 \frac{\mu_0 e}{m_e} \mathbf{P}_1 \times \mathbf{H}_1 - \frac{\omega_1^2}{en_0} \left(\mathbf{P}_1 \nabla \cdot \mathbf{P}_1 + \mathbf{P}_1 \cdot \nabla \mathbf{P}_1 - \mathbf{P}_1 \cdot \mathbf{P}_1 \frac{\nabla n_0}{n_0} \right) + \\ & + \frac{en_1}{m_e} \nabla \left(\frac{\delta G[n]}{\delta n} \right)_1 + \frac{en_0}{m_e} \nabla \left(\frac{\delta G[n]}{\delta n} \right)_2^{\text{NL}} \end{aligned} \quad (\text{S15})$$

The weak formulation of Eq. (S14) can be obtained by multiplying it with a test function $\tilde{\mathbf{P}}_j$ and integrating over the simulation domain.

$$\int \left[\frac{e}{m_e} \nabla \left(\frac{\delta G[n]}{\delta n} \right)_j + \frac{1}{n_0} \{ (\omega_j^2 + i\gamma\omega_j) \mathbf{P}_j + \varepsilon_0 \omega_p^2 \mathbf{E}_j \} + \frac{1}{n_0} \mathbf{S}_j \right] \cdot \tilde{\mathbf{P}}_j \, dV = 0 \quad (\text{S16})$$

$$\int -\frac{e}{m_e} \left(\frac{\delta G[n]}{\delta n} \right)_j (\nabla \cdot \tilde{\mathbf{P}}_j) + \frac{1}{n_0} [(\omega_j^2 + i\gamma\omega_j) \mathbf{P}_j + \varepsilon_0 \omega_p^2 \mathbf{E}_j] \cdot \tilde{\mathbf{P}}_j + \frac{1}{n_0} \mathbf{S}_j \cdot \tilde{\mathbf{P}}_j \, dV = 0 \quad (\text{S17})$$

Since $\mathbf{S}_1 = 0$, the integral of the nonlinear source (last) term in Eq. (S17) can be expressed as:

$$\begin{aligned} \int \frac{1}{n_0} \mathbf{S}_{\text{NL}} \cdot \tilde{\mathbf{P}}_2 \, dV = & \int \frac{1}{n_0} \left[\frac{e^2 n_1}{m_e} \mathbf{E}_1 + i\omega_1 \frac{\mu_0 e}{m_e} \mathbf{P}_1 \times \mathbf{H}_1 + \right. \\ & \left. - \frac{\omega_1^2}{en_0} \left(\mathbf{P}_1 \nabla \cdot \mathbf{P}_1 + \mathbf{P}_1 \cdot \nabla \mathbf{P}_1 - \mathbf{P}_1 \cdot \mathbf{P}_1 \frac{\nabla n_0}{n_0} \right) \right] \cdot \tilde{\mathbf{P}}_2 + \\ & + \frac{en_1}{m_e n_0} \nabla \left(\frac{\delta G[n]}{\delta n} \right)_1 \cdot \tilde{\mathbf{P}}_2 + \frac{e}{m_e} \nabla \left(\frac{\delta G[n]}{\delta n} \right)_2^{\text{NL}} \cdot \tilde{\mathbf{P}}_2 \, dV \end{aligned} \quad (\text{S18})$$

The last two terms appearing in the above equation emerge from the spatial dependence of the charge density. Thus, its weak form can be finally written as:

$$\begin{aligned} \int \frac{1}{n_0} \mathbf{S}_{\text{NL}} \cdot \tilde{\mathbf{P}}_2 \, dV = & \int \frac{1}{n_0} \left[\frac{e^2 n_1}{m_e} \mathbf{E}_1 + i\omega_1 \frac{\mu_0 e}{m_e} \mathbf{P}_1 \times \mathbf{H}_1 + \right. \\ & \left. - \frac{\omega_1^2}{en_0} \left(\mathbf{P}_1 \nabla \cdot \mathbf{P}_1 + \mathbf{P}_1 \cdot \nabla \mathbf{P}_1 - \mathbf{P}_1 \cdot \mathbf{P}_1 \frac{\nabla n_0}{n_0} \right) \right] \cdot \tilde{\mathbf{P}}_2 + \\ & - \frac{e}{m_e} \left(\frac{\delta G[n]}{\delta n} \right)_1 \left[\frac{n_1}{n_0} (\nabla \cdot \tilde{\mathbf{P}}_2) + \frac{1}{n_0^2} (n_0 \nabla n_1 - n_1 \nabla n_0) \cdot \tilde{\mathbf{P}}_2 \right] + \\ & - \frac{e}{m_e} \left(\frac{\delta G[n]}{\delta n} \right)_2^{\text{NL}} (\nabla \cdot \tilde{\mathbf{P}}_2) \, dV \end{aligned} \quad (\text{S19})$$

The advantage of the weak formulation is that there is no need to compute the gradients of the energy functionals and the derivatives are distributed to the test functions. The energy functionals also contain second-order derivative and we introduced working variables, such that, $\mathbf{F}_j = \nabla n_j$ where $n_j = \frac{1}{e} \nabla \cdot \mathbf{P}_j$ which implies that $\nabla \cdot \mathbf{F}_j = \nabla^2 n_j$. Thus, the complete set of nonlinear QHT equations, along with the two wave equations and a static QHT equation for computing equilibrium density, in their weak formulation reads,

$$\int (\nabla \times \mathbf{E}_j) \cdot (\nabla \times \tilde{\mathbf{E}}_j) - \left(\varepsilon_\infty \frac{\omega_j^2}{c^2} \mathbf{E}_j + \mu_0 \omega_j^2 \mathbf{P}_j \right) \cdot \tilde{\mathbf{E}}_j \, dV = 0 \quad (\text{S20})$$

$$\int -\frac{e}{m_e} \left(\frac{\delta G[n]}{\delta n} \right)_j (\nabla \cdot \tilde{\mathbf{P}}_j) + \frac{1}{n_0} [(\omega_j^2 + i\gamma\omega_j) \mathbf{P}_j + \varepsilon_0 \omega_p^2 \mathbf{E}_j] \cdot \tilde{\mathbf{P}}_j + \frac{1}{n_0} \mathbf{S}_j \cdot \tilde{\mathbf{P}}_j \, dV = 0 \quad (\text{S21})$$

$$\int -(\nabla \cdot \mathbf{P}_j) (\nabla \cdot \tilde{\mathbf{F}}_j) - e \mathbf{F}_j \cdot \tilde{\mathbf{F}}_j \, dV = 0 \quad (\text{S22})$$

$$\int -\varepsilon_\infty(\mathbf{r}) \nabla \left(\frac{\delta G[\xi^2]}{\delta n} \right)_{\xi=\sqrt{n_0}} \cdot \nabla \tilde{\xi} + \frac{e^2}{\varepsilon_0} (\xi^2 - n^+) \tilde{\xi} \, dV = 0 \quad (\text{S23})$$

where $j = 1, 2$ and $\mathbf{S}_1 = 0$. In Eq. (S23), the transformed variable $\xi = \sqrt{n_0}$ was introduced as in this way the solution converges more quickly.

[1] C. Ciraci and F. Della Sala, Phys. Rev. B **93**, 205405 (2016), ISSN 2469-9950, 2469-9969.
[2] K. A. O'Donnell and R. Torre, New J. Phys. **7**, 154 (2005), ISSN 1367-2630.
[3] COMSOL Multiphysics, <https://www.comsol.com>.